

See discussions, stats, and author profiles for this publication at: <https://www.researchgate.net/publication/24270261>

# NMR and Molecular Dynamics Study of the Binding Mode of Naphthalene-N-sulfonyl-D-glutamic Acid Derivatives: Novel MurD Ligase Inhibitors

ARTICLE in JOURNAL OF MEDICINAL CHEMISTRY · MAY 2009

Impact Factor: 5.45 · DOI: 10.1021/jm900117n · Source: PubMed

CITATIONS

12

READS

25

7 AUTHORS, INCLUDING:



Mihael Simcic

EN-FIST Centre of Excellence

9 PUBLICATIONS 104 CITATIONS

SEE PROFILE



Katja Kristan

University of Ljubljana

28 PUBLICATIONS 294 CITATIONS

SEE PROFILE



Uros Urleb

Sandoz

77 PUBLICATIONS 778 CITATIONS

SEE PROFILE



Simona Golič Grdadolnik

National Institute of Chemistry

110 PUBLICATIONS 1,313 CITATIONS

SEE PROFILE

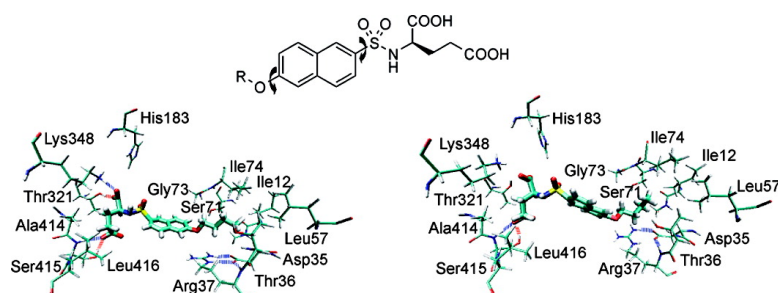
Article

## NMR and Molecular Dynamics Study of the Binding Mode of Naphthalene-*N*-sulfonyl-d-glutamic Acid Derivatives: Novel MurD Ligase Inhibitors

Mihael Simcic, Milan Hodoscek, Jan Humljan, Katja Kristan,  
Uros Urleb, Darko Kocjan, and Simona Golic Grdadolnik

*J. Med. Chem.*, **2009**, 52 (9), 2899-2908 • Publication Date (Web): 09 April 2009

Downloaded from <http://pubs.acs.org> on May 7, 2009



### More About This Article

Additional resources and features associated with this article are available within the HTML version:

- Supporting Information
- Access to high resolution figures
- Links to articles and content related to this article
- Copyright permission to reproduce figures and/or text from this article

[View the Full Text HTML](#)



**ACS Publications**  
High quality. High impact.

Journal of Medicinal Chemistry is published by the American Chemical Society,  
1155 Sixteenth Street N.W., Washington, DC 20036

# NMR and Molecular Dynamics Study of the Binding Mode of Naphthalene-*N*-sulfonyl-D-glutamic Acid Derivatives: Novel MurD Ligase Inhibitors

Mihael Simčič,<sup>#</sup> Milan Hodošček,<sup>‡</sup> Jan Humljan,<sup>†</sup> Katja Kristan,<sup>†</sup> Uroš Urleb,<sup>†</sup> Darko Kocjan,<sup>#,†</sup> and Simona Golič Grdadolnik<sup>\*,#</sup>

Laboratory of Biomolecular Structure and Laboratory of Molecular Modeling, National Institute of Chemistry, 1001 Ljubljana, Slovenia, and Drug Discovery, Lek Pharmaceuticals d.d., Verovškova 57, 1526 Ljubljana, Slovenia

Received January 29, 2009

The presented series of naphthalene-*N*-sulfonyl-D-glutamic acid derivatives are novel MurD ligase inhibitors with moderate affinity that occupy the D-Glu binding site. We performed an NMR study including transfer NOE to determine the ligand bound conformation, as well as saturation transfer difference experiments to obtain ligand epitope maps. The difference in overall appearance of the epitope maps highlights the importance of hydrophobic interactions and shows the segments of molecular structure that are responsible for them. Transfer NOE experiments indicate the conformational flexibility of bound ligands, which were then further examined by unrestrained molecular dynamics calculations. The results revealed the differing degrees of ligand flexibility and their effect on particular ligand–enzyme contacts. Conformational flexibility not evident in the crystal structures may have an effect on ligand-binding site adaptability, and this is probably one of the important reasons for the only moderate activity of novel derivatives.

## 1. Introduction

The bacterial peptidoglycan biosynthetic pathway consists of several steps that are considered as targets for the development of novel antimicrobial agents. Mur ligases are intracellular enzymes involved in the biosynthesis of cytosolic peptidoglycan precursors. In particular, MurA and MurB enzymes catalyze the synthesis of UDP-*N*-acetylmuramic acid (UDP-MurNAc<sup>o</sup>), while MurC to MurF enzymes consecutively link peptides L-Ala, D-Glu, L-Lys, and D-Ala-D-Ala dipeptide, respectively, to form UDP-MurNAc-pentapeptide. Subsequently, the pentapeptide is attached to a lipid tail and further cross-linked within the cell membrane.<sup>1,2</sup>

A paper<sup>3</sup> recently appeared on novel naphthalene-*N*-sulfonyl-D-glutamic acid derivatives that inhibit MurD, a key enzyme within the Mur ligase series. The IC<sub>50</sub> values of a structurally diverse set of compounds ranging between 80 and 600  $\mu$ M did provide some foundation for the structure–activity relationship. It appears that the best inhibitor has a 2-naphthalene substituted *N*-sulfonyl-D-glutamic acid and arylalkyloxy substituent at the 6- and 7-positions. SAR indicates that the 6-(aryl)alkyloxynaphthalene side chain contributes favorably to the binding affinity, and the lipophilic character makes the dominant contribution.

It is interesting to note that MurD was shown to be highly stereospecific when D,L-Glu enantiomers were used as substrates. L-Glu is completely inactive up to 5 mM.<sup>5</sup> However, enzyme

stereospecificity is much less pronounced with regard to inhibition by naphthalene-*N*-sulfonyl-D,L-glutamic acid derivatives. For example, (*R*)- and (*S*)-6-butoxy derivatives give an IC<sub>50</sub> ratio of only 2.5.<sup>4</sup>

The high resolution crystal structure of the MurD complex with several inhibitors revealed detailed inhibitor binding within the active site. Most notably, the glutamate moiety of the naphthalene-*N*-sulfonyl-D,L-glutamic acid derivatives binds within the D-Glu-binding pocket. The naphthalene ring of the inhibitors is positioned in a cleft within the binding site, possibly making hydrophobic interactions, and the 6-(aryl)alkyloxy substituents extend into the uracil-binding pocket. It seems that only small differences in the binding modes of the naphthalenesulfonamido group contributed to the 3-fold difference in IC<sub>50</sub> values between (*R*)- and (*S*)-6-butoxy derivatives. Moreover, positional isomers, 6-(4-cyanobenzyloxy)naphthalene derivative and the analogous 7-derivative, show comparable IC<sub>50</sub> values. A comparison of high resolution crystal structures of the MurD complex with both compounds indicates that the binding site can easily accommodate both conformations of the lipophilic moieties.<sup>3</sup> There is no doubt that the experimentally determined positions and conformations of compounds in the MurD active site offer a solid foundation for optimization of inhibitors in this structural class.

However, we considered that the exploration of conformational dynamics of the ligands in the enzyme binding site might shed some additional light on the 3D static pictures yielded by X-ray diffraction. It is generally accepted that conformational dynamics can strongly affect the stability of the ligand–protein complex. In view of the concepts on induced fit or protein conformation selection, which focus on ligand–protein binding site adaptability,<sup>6</sup> a conformational dynamics study could afford important findings that complement the conclusions from the SAR study and the high resolution crystal structure studies. Moreover, the crystal structures of several novel derivatives in complex with MurD could not be determined. For the novel

\* To whom correspondence should be addressed. Phone: +386 1 4760 409. Fax: +386 1 4760 300. E-mail: simona.grdadolnik@ki.si.

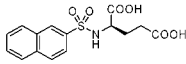
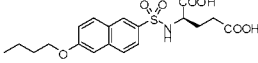
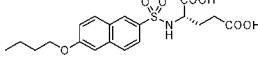
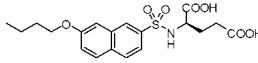
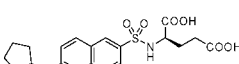
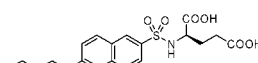
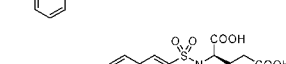
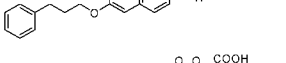
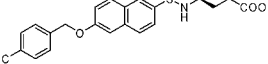
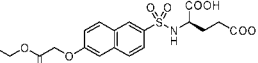
<sup>#</sup> Laboratory of Biomolecular Structure, National Institute of Chemistry.

<sup>‡</sup> Laboratory of Molecular Modeling, National Institute of Chemistry.

<sup>†</sup> Lek Pharmaceuticals d.d.

<sup>a</sup> Abbreviations: UDP, uridine 5'-diphosphate; UDPMurNAc, uridine diphosphate-*N*-acetylmuramic acid; MurA, UDP-*N*-acetylglucosamine enolpyruvyl transferase; MurB, UDP-*N*-acetylpyruvylglucosamine reductase; MurC, UDP-*N*-acetylmuramate/L-alanine ligase; MurD, UDP-*N*-acetylmuramoyl-L-alanine/D-glutamate ligase; MurE, UDP-*N*-acetylmuramoyl-L-alanyl-D-glutamate/*meso*-diaminopimelate ligase; MurF, UDP-*N*-acetylmuramoyl-L-alanyl- $\gamma$ -D-glutamyl-*meso*-diaminopimelate/D-alanyl-D-alanine ligase; NOE, nuclear Overhauser effect; NOESY, nuclear Overhauser effect correlation spectroscopy; STD, saturation transfer difference; MD, molecular dynamics.

**Table 1.** Structures of Investigated Compounds<sup>a</sup>

		IC <sub>50</sub> (μM)
<b>11d</b>		810
<b>17c</b>		280
<b>20</b>		710
<b>38</b>		180
<b>17i</b>		400
<b>17j</b>		239
<b>17k</b>		132
<b>17l</b>		105
<b>17f</b>		192
<b>17g</b>		630

<sup>a</sup> MurD inhibitory activity of compounds was published previously. The same compound labels are used as in the published synthetic studies.<sup>3</sup>

inhibitors examined in this study (Table 1) only the crystal structures of **17c**, **20**, and **17l** in complex with MurD are available.<sup>3,4</sup>

Here we report the results of the solution NMR and unrestrained molecular dynamics (MD) studies of a series of novel naphthalene-*N*-sulfonyl-D,L-Glu derivatives (Table 1) in complex with MurD. For the NMR studies MurD (47.7 kDa) was isolated and purified from *E. coli*. Because of the high molecular weight of the enzyme and moderate binding affinity of novel derivatives, ligand-based NMR methods, transferred NOE, and saturation transfer difference experiments were selected to investigate the bound ligands. The aim was to obtain the conformational and dynamic properties of the bound ligands and to explore their influence on ligand–enzyme interactions. This will provide structural and dynamic insight into the observed differences in the activity of novel inhibitors, which could be important for the rational design of more active derivatives.

## 2. Results and Discussion

**2.1. Conformation of the Bound Ligands.** The conformational properties of the bound naphthalene-*N*-sulfonyl-D,L-Glu derivatives were studied by the application of transferred NOE experiments.<sup>7,8</sup> Initial NOE experiments of the most potent derivatives performed in the absence and in the presence of MurD have shown that the rate of dissociation from the complex fulfils the requirements for successful transfer of NOEs from

the bound to the free state. The sign change of the ligand NOE cross-peaks was observed upon addition of the enzyme. In NOESY spectra recorded in the absence of the enzyme only a few very weak positive NOE cross-peaks were observed. Thus, the contribution of the NOE contacts of the free ligand to the transferred NOE cross-peaks is negligible.

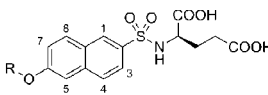
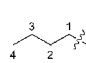
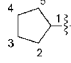
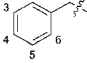
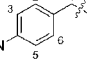
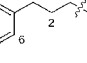
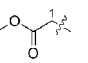
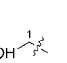
Nontrivial NOEs observed in transferred NOESY spectra and calculated distances are listed in Table 2. Distances from the crystal structures<sup>3,4</sup> are added for the derivatives **17c**, **20**, and **17l**. For some derivatives mutually exclusive NOEs are observed between the naphthalene ring and its C6 or C7 substituent and between the naphthalene ring and D-Glu moiety. These NOEs indicate the conformational dynamics of the ligands at the enzyme binding site. Because of the conformational averaging, the NOEs will be used qualitatively as indicators for the presence or absence of a population with a certain type of relative orientations between molecular segments. The differences in distance values can be a consequence of different population distributions between exchanging conformers in solution. The distance values in Table 2 are given just to emphasize the differences between the conformational properties of bound ligands in the crystal and in solution.

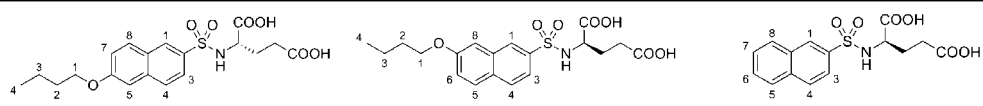
Strong NOEs between H5 and CH<sub>2</sub>(1) are observed for C6 substituted naphthalene-*N*-sulfonyl-D,L-Glu derivatives. Weak NOEs between H7 and CH<sub>2</sub>(1) protons are also present for most of the derivatives. Simultaneous observation of H5–CH<sub>2</sub>(1) and H7–CH<sub>2</sub>(1) NOEs could be a consequence of naphthalene ring rotation or different orientations of the C6 substituent. In the case of derivative **17i**, similar conformation flexibility can be proposed because of the presence of mutually exclusive H5–cPeH1 and H7–cPeH1 NOEs. An additional pair of mutually exclusive NOEs of H5 with cyclopentyl cPeH2 and cPeH5 protons indicates cyclopentyl ring rotation (Figure 1). NOEs that would indicate rotations of the phenyl or cyanobenzyl ring of derivatives **17j**, **17k**, and **17l** cannot be observed because of the magnetic equivalence of protons at the ortho and meta positions of the free ligand. For the C7 substituted *N*-sulfonyl-D-Glu derivative (**38**), conformational flexibility in this part of the molecule can be proposed because of observations of strong H8–CH<sub>2</sub>(1) and weak H6–CH<sub>2</sub>(1) NOEs.

The proximity of H5 and CH<sub>2</sub>(1) protons is observed only in the crystal structure of bound **17c**. In the crystal structures of bound **20** and **17l** these protons are more than 4 Å apart while the H7 and CH<sub>2</sub>(1) protons are closer than 2.6 Å. Differences in these distances indicate a different orientation of the alkyloxy moiety relative to the naphthalene ring. In solution, the preferred orientation of the alkyloxy moiety relative to the naphthalene ring appears to be similar for all C6 substituted derivatives with IC<sub>50</sub> values ranging between 100 and 710 μM.

Naphthalene ring rotation can also cause the mutual appearance of H3–H<sup>α</sup> and H1–H<sup>α</sup> NOEs. For D-Glu derivatives, medium H1–H<sup>α</sup> NOEs, and medium (**17c**, **17l**, **17k**, **11d**) or weak (**17i**, **17j**, **17f**, **17g**, **20**, **38**) H3–H<sup>α</sup> NOEs are observed. The relative orientation of the D-Glu moiety and naphthalene ring in the crystal structures of bound **17c** and **17l** corresponds only to the observation of the H3–H<sup>α</sup> NOE. For the L-Glu derivative (**20**), both NOEs between the naphthalene ring protons and the H<sup>α</sup> proton are weak. This is the only significant difference between bound conformations of the more potent D-Glu derivatives and the less potent L-Glu derivative in solution that is obviously influencing the ligand–enzyme interactions. In the crystal structure of bound **20** the H3–H<sup>α</sup> and H1–H<sup>α</sup> distances are larger than 4.3 Å. The formation of an extended

**Table 2.** Nontrivial NOE Connectivities and Corresponding Distances (Å) Calculated from Transferred NOESY Spectra

<div></div>							
R	<div></div>	<div></div>	<div></div>	<div></div>	<div></div>	<div></div>	<div></div>
label	17c	17i	17j	17l	17k	17f	17g
H1 - H <sup>α</sup>	3.2 4.7 <sup>a</sup>	3.0	3.1	3.1 4.5 <sup>d</sup>	2.9	2.9	3.6
H3 - H <sup>α</sup>	3.1 2.5 <sup>a</sup>	3.6	weak <sup>b</sup>	3.5 2.3 <sup>d</sup>	3.1	4.4	weak <sup>b</sup>
H5 - CH <sub>2</sub> (1)	2.4 2.4 <sup>a</sup>		2.4	2.4 4.2 <sup>d</sup>	strong <sup>c</sup>	2.4	2.3
H7 - CH <sub>2</sub> (1)	3.8 4.3 <sup>a</sup>		weak <sup>c</sup>	weak <sup>c</sup> 2.2 <sup>d</sup>	weak <sup>c</sup>	weak <sup>c</sup>	no
H5 - cPeH1		2.6					
H7 - cPeH1		3.8					
H5 - cPeH2		3.5					
H5 - cPeH5		3.5					

<div></div>			
label	20	38	11d
H1 - H <sup>α</sup>	3.7 4.4 <sup>e</sup>	2.9	3.1
H3 - H <sup>α</sup>	4.0 5.0 <sup>e</sup>	3.9	3.4
H5 - CH <sub>2</sub> (1)	2.5 4.3 <sup>e</sup>		
H7 - CH <sub>2</sub> (1)	4.0 2.5 <sup>e</sup>		
H6- CH <sub>2</sub> (1)		4.1	
H8- CH <sub>2</sub> (1)		2.6	

<sup>a</sup> Distance from X-ray structure, PDB code 2jff.<sup>4</sup> <sup>b</sup> Observed in 1D trace from 2D spectrum. <sup>c</sup> Overlapped. <sup>d</sup> Distance from X-ray structure, PDB code 2uup.<sup>3</sup> <sup>e</sup> Distance from X-ray structure, PDB code 2jfh.<sup>4</sup>

ring-type system is observed in the *N*-sulfonyl-D-Glu moiety in the crystal structures of **17c** and **17l**, which is absent in the crystal structure of **20**.<sup>3,4</sup> For D-Glu derivatives with IC<sub>50</sub> values ranging from 105 to 810 μM both orientations of the naphthalene ring relative to the D-Glu moiety are populated in solution, and the orientation corresponding to the proximity of H1 and H<sup>α</sup> protons is more favorable.

**2.2. Ligand Epitope Mapping.** Saturation transfer difference (STD) NMR<sup>9,10</sup> was used to investigate ligand–enzyme contacts. STD amplification factors for epitope mapping were determined with a short saturation delay of 350 ms to avoid the effect of the longitudinal relaxation rate on the signal intensities. Nonuniform relaxation properties across the molecule are observed for all derivatives. The <sup>1</sup>H *T*<sub>1</sub> relaxation times in

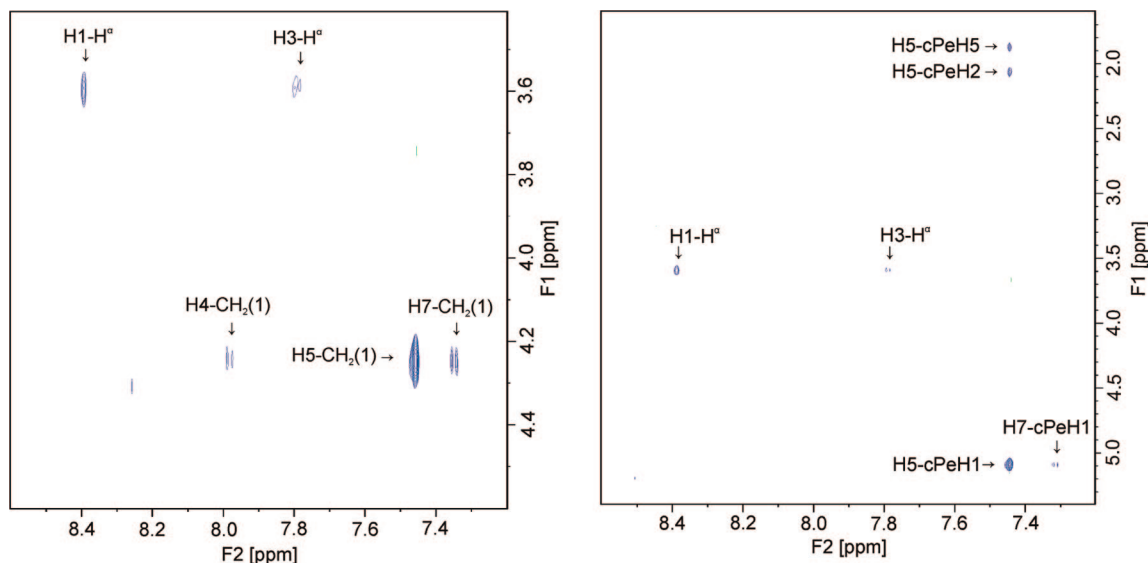


**Figure 1.** Expanded regions of NOESY spectra of compounds **17c** (left) and **17i** (right) showing the presence of mutually exclusive NOEs. The H4-CH<sub>2</sub>(1) cross-peak (left) is most probably a consequence of spin diffusion across the H5 proton.

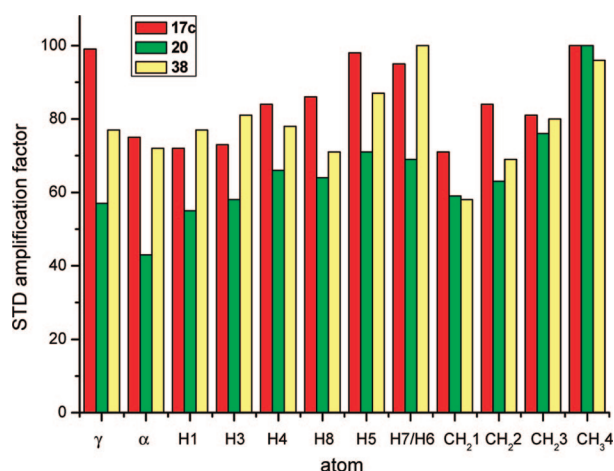


**Figure 2.** Relative degrees of saturation of individual protons of derivatives **17c** (red), **20** (green), and **38** (yellow) determined from 1D STD NMR spectra at a 97-fold excess. The values in each molecule are normalized to the intensity of the signal with the largest STD effect.

the naphthalene ring are in the range from 1.4 to 3.0 s. The lowest  $T_1$  values between 0.7 and 0.9 s are observed for protons in the Glu moiety, while the highest  $T_1$  values between 3.3 and 4.4 s are found for protons in the phenyl ring of the arylalkoxy substituents. A saturation period shorter than half of the shortest  $T_1$  is recommended to eliminate the effect of relaxation on STD amplification factors.<sup>11</sup> The sensitivity under short saturation conditions is greatly reduced. Therefore, STD amplification factors could not be determined for some multiplet signals of low intensity, especially for  $\beta$ -protons. These protons have  $T_1$  relaxation times lower than 0.8 s, while the  $T_1$  of other protons is equal to or higher than 0.8 s.

Note that in the STD ligand epitope maps (Figures 2–4) the relative values of the STD amplification factor are normalized in each molecule separately. The strength of interactions with the protein can be compared only between the atoms inside a particular molecule. The STD amplification factor is not an appropriate parameter for intermolecular comparison because its magnitude depends on the exchange kinetics of the ligand.<sup>10</sup>

A major difference in overall appearance of the STD epitope maps of D- and L-Glu butoxy derivatives (compounds **17c**, **38**,

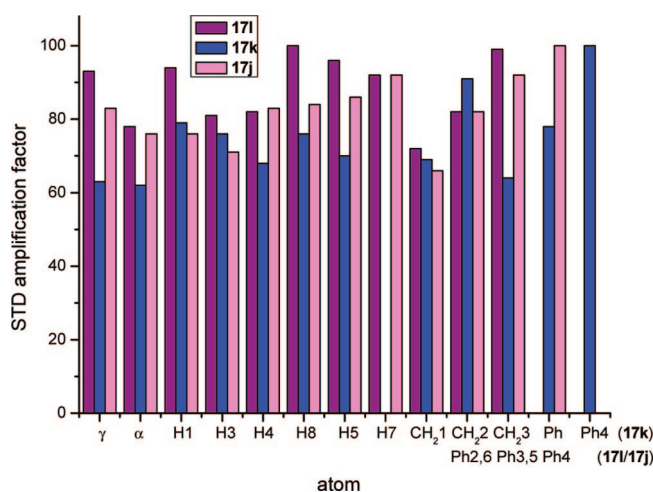


**Figure 3.** Relative degrees of saturation of individual protons of derivatives **17i** (purple), **17k** (blue), and **17j** (magenta) determined from 1D STD NMR spectra at a 97-fold excess. The values in each molecule are normalized to the intensity of the signal with the largest STD effect.

and **20**) represents the relative strength of the STD effect in the butoxy chain with respect to the rest of the molecule (Figure 2). The 3-fold reduced activity of the L-Glu derivative (**20**) seems to be a consequence of less favorable interactions of the L-Glu moiety and naphthalene ring with the enzyme. The methyl protons of the lipophilic butoxy substituent of **20** have a significantly stronger STD effect than the protons in the other segments of the molecule. On the basis of the crystal structures of MurD in complex with **17c** and **20**, the less favorable binding interactions of **20** have been proposed because of the displacement of its naphthalenesulfonamido group in the binding cleft. The D-Glu derivatives (**17c** and **38**) have a uniform STD effect across the molecule. A similar proximity of protons to the enzyme in all three molecular segments is observed, especially for the C6 substituted D-Glu derivative **17c**. The relative strength of interactions of butoxy chain and naphthalene ring with respect to D-Glu is slightly increased for the C7 substituted derivative **38**. It seems that C7 substitution strengthens the hydrophobic contacts of the ring and butoxy chain with the enzyme.



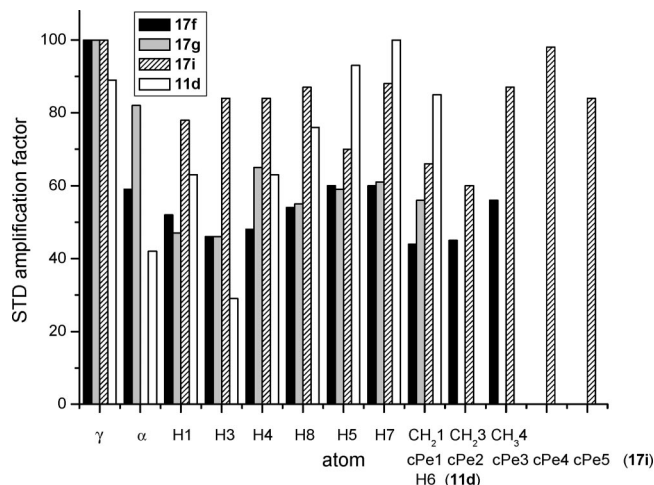


**Figure 4.** Relative degrees of saturation of individual protons of derivatives **17f** (black), **17g** (gray), **17i** (striped), and **11d** (white) determined from 1D STD NMR spectra at a 97-fold excess. The values for each molecule are normalized to the intensity of the signal with the largest STD effect.

In general, the arylalkyloxy derivatives **17k** and **17j** with increased lipophilicity of the C6 substituent and its overall bulkiness yield similar epitope maps (Figure 3). The protons with the highest degree of STD effect, which are in tightest contact with the protein, are located in the C6 substituents. However, the relative strength of the hydrophobic contacts of the C6 substituent with respect to the interactions of the rest of the molecule is higher for **17k** than **17j**. An almost 2-fold increased activity of **17k** in comparison to **17j** confirms the importance of hydrophobic contacts within the uracil-binding pocket. For cyanobenzoyloxy derivative **17i** more uniform STD effects across the molecule are observed (Figure 3). This cannot be attributed to less favorable interactions of the C6 substituent because the C4 substitution of the phenyl ring with a cyano group prevents observation of the STD effect at the ring's para position. The crystal structure of the **17i**–MurD complex reveals the various interactions of the cyanobenzoyloxy substituent with the uracil binding pocket, i.e., hydrogen bonding and  $\pi$ – $\pi$  stacking, which obviously increases its activity more than 2-fold with respect to **17j**.

For derivatives **17f**, **17g**, and **17i** (Figure 4) the largest STD effects are observed in the D-Glu moiety. It seems probable that the absence of the methylene spacer in the cyclopentylloxy substituent (**17i**) reduces the contacts of this lipophilic substituent with hydrophobic residues in the uracil binding pocket, and therefore, the contacts between the D-Glu and C6 substituent protons turn out to be similar. Consequently, there is an almost 2-fold and 3-fold reduced activity of **17i** with respect to arylalkyloxy derivatives **17k** and **17l**. The relative strength of the STD effects in the C6-substituent is largely reduced for derivatives **17f** and **17g**. Introduced polarity in the C6 substituents of **17f** and **17g** obviously reduces hydrophobic contacts with the uracil binding pocket. In addition, the relative strength of the STD effect in the naphthalene ring is also reduced in comparison to D-Glu butoxy and arylalkyloxy derivatives. A similar effect was observed for L-Glu derivative **20**. Significantly lower activity of derivatives **17g** and **20** shows the importance of naphthalene ring interactions. On the other hand the loss of hydrophobic contacts in **17f** does not affect its activity, which is even slightly higher than that of **17c**. One possible explanation for this effect could be the formation of hydrogen bonds by its C6 substituent with the receptor binding site.

Surprisingly, the strongest STD effect of unsubstituted naphthalenesulfonamide **11d** is observed in the naphthalene ring and not in the D-Glu moiety (Figure 4). We can speculate that interactions of naphthalene ring substituents with the uracil binding site are hindering the enzyme–naphthalene ring interactions of derivatives **17f**, **17g**, and **17i**. However, the complete lack of interactions with the uracil binding pocket of **11d** results in the lowest activity among the investigated compounds (Table 1).

**2.3. Molecular Dynamics at the Receptor Level.** Unrestrained molecular dynamics simulations of ligand–MurD complexes clearly indicate the conformational flexibility of naphthalene-*N*-sulfonyl-D,L-Glu derivatives at the MurD binding site. During simulations the naphthalene ring rotates around its C2–C6 axis by up to 180° and conformational flexibility connected with reorientation of the alkyloxy moiety or ring rotations in C6/C7 substituents is observed. During naphthalene ring rotations notable changes in H1–H $\alpha$  and H3–H $\alpha$  distances appear. A particular orientation of the naphthalene ring corresponds to proximity of H1–H $\alpha$  or of H3–H $\alpha$  protons. For **20**, these protons are in general more than 3.5 Å apart during the simulation, which is in agreement with NOE studies. In most cases, the dihedral angle C5–C6–O–CH<sub>2</sub>(1) also significantly changes during pronounced reorientation of the naphthalene ring. Therefore, the substituent remains fixed in the uracil binding site, while only the naphthalene ring reorients. However, in some cases the C5–C6–O–CH<sub>2</sub>(1) dihedral angle is stable and changes in the dihedral angles of the alkyloxy moiety, which are more remote from the naphthalene ring, appear. Significant changes in the dihedral angles in the alkyloxy moiety and ring rotations in the substituent can also be observed in the trajectories when the naphthalene ring position is stable and indicate additional conformational flexibility of the substituents, which is not connected with naphthalene ring rotations. With pronounced changes in the dihedral angle C5–C6–O–CH<sub>2</sub>(1), distances between the CH<sub>2</sub>(1) protons and H5 or H7 protons change such that either H5 or H7 is closer to the methylene protons. Conformational flexibility of the derivatives observed during MD simulation is thus consistent with the observation of mutually exclusive NOEs discussed in section 2.1.

Different extents of naphthalene ring flexibility observed in MD trajectories of butoxy derivatives (**17c**, **20**, and **38**) are a major reason for dissimilarities in the binding mode of these derivatives. The most pronounced naphthalene ring reorientations up to 180° are observed several times during 2 ns of simulations for L-Glu derivative **20** (Figure 5A). These severely affect the electrostatic interactions of the L-Glu moiety with the enzyme. Only hydrogen bonds between the  $\gamma$ -carboxyl group and Ser415 are formed during entire simulation, while hydrogen bonds with Phe422 and Arg425 are lost after ring reorientation at 900 ps. Hydrogen bonds of the  $\alpha$ -carboxyl group with Lys348 and Thr321 are disturbed at 900 ps and finally lost after the ring flips over at 1600 ps. On the other hand, the  $\alpha$ -carboxyl group of D-Glu derivatives **17c** and **38** forms hydrogen bonds with Lys348 and Thr321 for almost the entire simulation. The  $\gamma$ -carboxyl groups of **17c** and **38** have stable hydrogen bonds with Ser415. In addition, the  $\gamma$ -carboxyl group of **17c** has an unstable but frequently formed hydrogen bond with Phe422. Less pronounced naphthalene ring rotations along the trajectories of **17c** and **38** (Figure 5B,C) do not affect hydrogen bonding of the D-Glu moiety with the enzyme.

Fewer hydrogen bonds are observed in solution than in the crystal structure of **17c**–MurD and **20**–MurD complexes.<sup>4</sup> This is expected, as many of them were formed across conserved

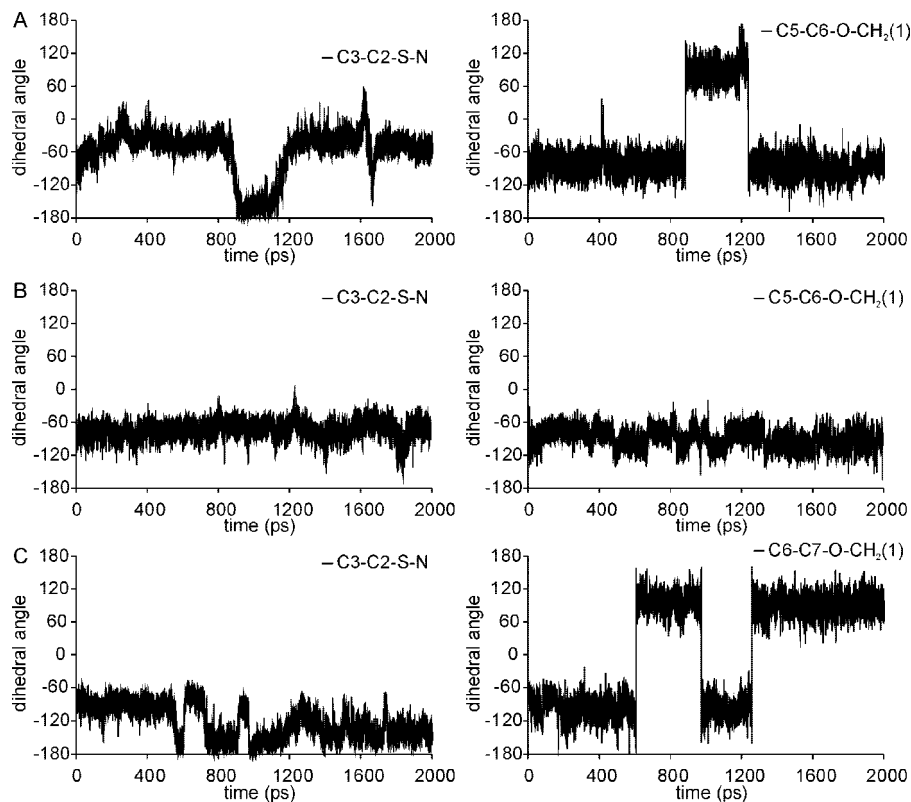


**Figure 5.** Dihedral angles C3–C2–S–N (left) and C5–C6–O–CH<sub>2</sub>(1) (right) along MD trajectories of **20** (A), **17c** (B), and **38** (C), indicating rotations of naphthalene ring and flexibility in the alkyl chain.

water molecules in the crystal structure. The hydrogen bonds of the sulfonic moiety, which are absent in solution complexes, were formed exclusively across water molecules. Direct hydrogen bonds of the D-Glu moiety with the enzyme are also observed in MD simulations where differences in their stability occur. Moreover, MD simulations show formation of a direct hydrogen bond between the  $\alpha$ -carboxyl group and Thr321. In crystal structures, this ligand–enzyme contact is formed across a conserved water molecule. Interestingly, direct interaction between the  $\alpha$ -carboxyl group and Thr321 is also observed in the crystal structure of the UMAG–MurD complex.<sup>12</sup>

Hydrophobic interactions in **20**–MurD complex are not as connected to the flexible naphthalene ring and are more stable than electrostatic interactions. The alkyl chain remains positioned between Ser71, Gly73, Ile74, Ile12, Gly12, Asp35, Thr36, and Arg37 during the entire simulation. This is in agreement with the STD ligand epitope map of **20** (Figure 2), which indicates the closest ligand–enzyme contact for protons in the alkyl chain. The naphthalene ring is positioned between Pro72, Gly73, Phe161, and Leu416, probably making hydrophobic contact. Proximity with Leu416 and Phe161 is lost during the first 200 ps. Proximity of the ring to Pro73 and Gly73 is observed during almost the entire simulation. Only between 900 and 1200 ps, during the other orientation of the ring, is Pro73 more remote, but Leu416 is again in spatial proximity. The alkyl chain of **17c** has a similar position in the uracil binding site as that of **20**. Close hydrophobic contacts between the naphthalene ring and Pro72, Gly73, and Leu416 are present during the entire simulation. In contrast to **17c**, the alkyl chain of the C7-substituted butoxy derivative **38** is much more flexible within the uracil binding pocket. Some of its hydrophobic contacts are stabilized only after 1.5 ns of simulation. Proximity of the alkyl chain and naphthalene ring with Gly73 exists during the entire simulation. Leu416 is more remote from the naphthalene ring

than in the **17c**–MurD complex. Close contacts with Pro72 and Phe161 are lost during the first reorientation of the ring; afterward these two residues are at a similar distance as Leu416.

The almost 3- to 4-fold reduced activity of L-Glu derivative **20** with respect to D-Glu isomeric 6-, 7-butoxy derivatives **17c** and **38** can be mainly attributed to the significantly higher naphthalene ring flexibility, which considerably destabilizes the electrostatic interactions of the L-Glu moiety with the enzyme. Hydrophobic contacts of the enzyme with the alkyl chain are less sensitive to ring rotations.

Although polarity was introduced in the alkyloxy substituent of **17f**, which is unfavorable for hydrophobic contacts with the uracil binding site, this derivative has a higher activity than **17c**. MD simulation of the **17f**–MurD complex indicates the formation of a hydrogen bond between the carbonyl group (C(2), Table 2) of the substituent and the Ser71 hydroxyl group (Figure 6). In addition, close hydrophobic contacts of the methyl and methylene groups with Gly73, Ile74, Ile12, Gly12, and Thr36 are present during the entire simulation, as seen in the butoxy derivatives. A combination of hydrophobic interactions and hydrogen bonding between the C6 substituent and the uracil binding site is obviously favorable for the activity of derivative **17f**. Two naphthalene ring rotations of approximately 100° occur between 1 and 1.4 ns of simulation; after that the frequently populated hydrogen bond of the substituent and stable hydrogen bond of the  $\alpha$ -carboxyl group with Lys348 are lost. The proximity of the naphthalene ring with Pro72 and Gly73 is not affected, while proximity to the Phe161 and Leu416 changes; the first one becomes closer and the second one more remote.

A more than 3-fold reduced activity of **17g** with respect to **17f** can be attributed to the complete lack of hydrophobic contacts by its highly polar substituent, which are not replaced by hydrogen bonds (Figure 6). Only during the first 300 ps are hydrogen bonds between substituent carboxyl group and Arg37



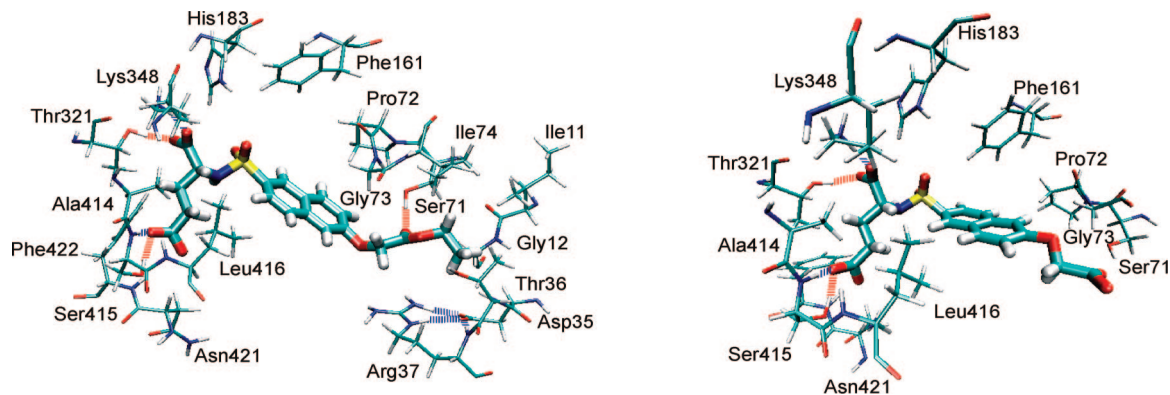


**Figure 6.** Snapshots from MD trajectories showing the binding mode of derivative **17f** (left) and **17g** (right) in the MurD binding site.

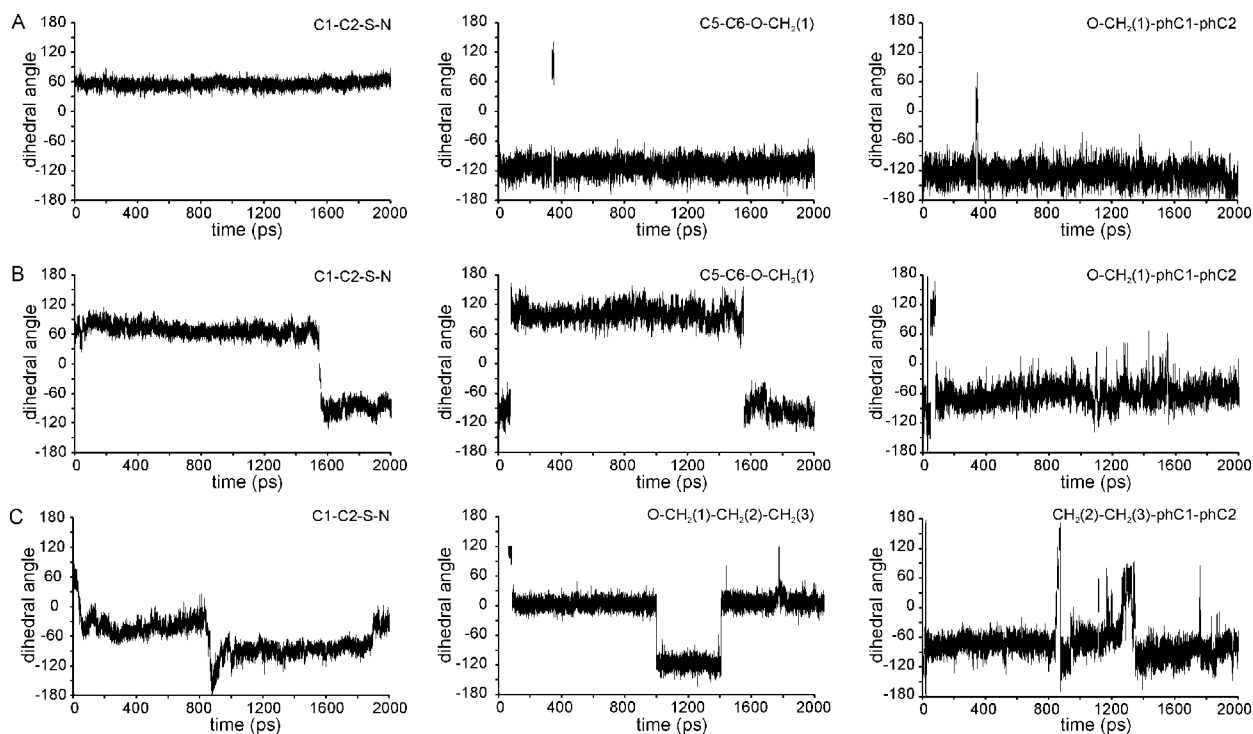


**Figure 7.** Dihedral angles C1–C2–S–N (left), C5–C6–O–CH<sub>2</sub>(1) or O–CH<sub>2</sub>(1)–CH<sub>2</sub>(2)–CH<sub>2</sub>(3) (middle), and O–CH<sub>2</sub>(1)–PhC1–PhC2 or CH<sub>2</sub>(2)–CH<sub>2</sub>(3)–PhC1–PhC2 (right) along MD trajectories of **17i** (A), **17j** (B), and **17k** (C), indicating naphthalene ring rotations, flexibility in alkyloxy moiety, and phenyl ring rotations.

formed, which are then lost during the significant reorientation of the naphthalene ring. Because of unfavorable interactions, the proximity of the **17g** substituent with the residues of the uracil binding site, otherwise present in complexes of more active alkyloxy and aralkyloxy derivatives, is lost.

During 2 ns of simulations, the naphthalene ring of aralkyloxy derivative **17i**, which is the most active of the investigated compounds, is by far the most stable (Figure 7A). Pronounced conformational flexibility of **17i** is observed only in the C6 substituent around 350 s, where simultaneous rotation in the alkyloxy moiety and a 180° flip of cyanobenzyl ring appear (Figure 7A). This does not affect the proximity of the ring to Asp35 and Arg37 and therefore any possible  $\pi$ – $\pi$  interaction between the ring and salt bridge of these two residues. Proximity of the ring with Thr36 is also undisturbed. However, the hydrogen bond between Thr36 and the cyano group observed in the crystal structure is not formed. Possible  $\pi$ – $\pi$  interaction is a crucial difference with respect to the alkyloxy derivatives, since proximity of the cyanobenzyl ring with the same residues of uracil binding site is observed as for

alkyl chains. The naphthalene ring of **17i** is in proximity to Gly73, Phe61, and Leu416 as in the crystal structure. The  $\alpha$ -carboxyl group has a stable hydrogen bond with Lys348 and an unstable frequently formed hydrogen bond with Thr321. In the crystal structure, the hydrogen bond with Thr321 is formed across the water molecule. The  $\gamma$ -carboxyl group has stable hydrogen bonds with Ser415 and an unstable but frequently formed hydrogen bond with Phe422.

Naphthalene ring reorientations of 150° and 60° are observed for less active aralkyloxy derivatives **17j** and **17k** (Figure 7B,C). It seems that these rotations are coupled with increased fluctuations in the phenyl ring orientation, which introduce instability into the contacts of the phenyl ring with the uracil binding site. This is more pronounced for **17j** than for **17k**. An approximately 2-fold reduced activity of **17j** with respect to **17k** and **17i** can also be attributed to the reduced number of hydrophobic contacts of the **17j** phenyl ring with the uracil binding site and a more remote position with respect to Asp35 and Arg 37 (Figure 8). The rotation of the naphthalene ring by 150° in **17j** appears after larger phenyl ring fluctuations. At

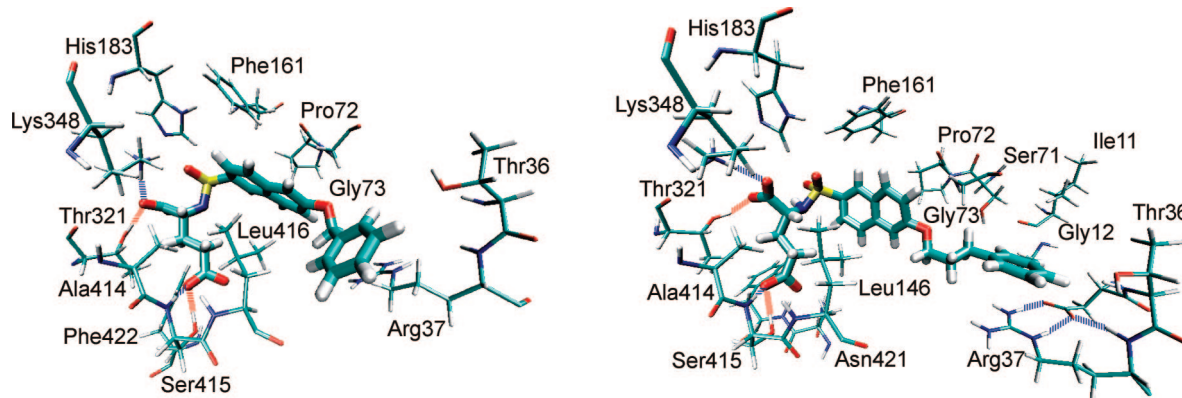


**Figure 8.** Snapshots from MD trajectories showing the binding mode of derivatives **17j** (left) and **17k** (right) in the MurD binding site.

naphthalene ring reorientations of 60°, a 180° degree flip of the phenyl ring of **17k** appears followed by larger fluctuations in its orientation. During this period the proximity with Asp35 and Arg37 is destabilized. Reorientations of the naphthalene ring in **17j** and **17k** disturb its hydrophobic contacts only for a short time; otherwise the proximity with Pro72, Gly73, Phe161, and Leu416 is present during the entire simulation. The hydrogen bonding network of the D-Glu moiety of **17j** and **17k** with the enzyme is not affected by naphthalene ring rotations and is similar to **17i**. However, there are a few differences: the formation of an unstable hydrogen bond between the  $\gamma$ -carboxyl group of **17k** and Arg425 not observed for **17i** and **17j** and the absence of a hydrogen bond between the  $\gamma$ -carboxyl group and Phe422 of **17j**.

During pronounced reorientation of the naphthalene ring in cyclopentyl derivative **17i**, the cyclopentane ring rotates simultaneously. This probably reduces the strength of the hydrophobic contacts with the uracil binding site and may explain the almost 2-fold reduced activity with respect to **17j**. The phenyl ring of **17j** remains positioned in the uracil binding site during naphthalene ring rotation. Otherwise the same residues of the uracil binding site are in proximity to both substituents. The reduced strength of the hydrophobic contacts of the **17i** substituent with respect to the **17j** substituent is also observed in the STD epitope maps. The STD effects of the phenyl ring are larger than in other parts of **17j**, while the STD effects of the cyclopentane ring are lower than those of D-Glu moiety of **17i** (Figures 3 and 4). In contrast to arylalkyl derivatives, large variations in the C2–S–N–CA dihedral angle are observed during naphthalene rotation, which disturb its proximity with Pro72, Phe161, and Leu416. In the case of **17j** this proximity is stable during the entire simulation. A similar hydrogen bonding network in the D-Glu moiety is observed as for **17j**, only the hydrogen bond with Thr321 is less stable.

Surprisingly, for unsubstituted naphthalenesulfonamide **11d** significant rotations of the naphthalene ring around its C2–C6 axis are not observed. However, large variations in the C2–S–N–CA dihedral angle occur, which are related to in-plane rotations of the ring by up to 60°. Interestingly close contacts between the ring and Pro72, Gly73, and Phe161 on one side and Leu416 on the other side are stable during the entire simulation. Obviously the naphthalene ring binding site adapts to such a ligand and prevents ring rotations around the C2–C6 axis. It seems that the uracil binding site interactions with the substituent hinder the optimal fit of the naphthalene ring binding site. When the strength of the naphthalene ring–MurD hydrophobic contacts are reduced, ring rotations appear, which destabilize other ligand–MurD contacts. Firm

interactions of the naphthalene ring of **11d** are in agreement with its STD ligand epitope map, where the strongest STD effect appears in the naphthalene ring (Figure 4). In contrast to substituted naphthalenesulfonamides a frequently formed hydrogen bond between the sulfonic group and Asn128 is observed. The D-Glu moiety of **11d** forms stable hydrogen bonds with Ser415 and Lys348 and unstable but frequently populated hydrogen bonds with Thr321 and Phe422.

### 3. Conclusions

The conformational properties of the bound naphthalene-*N*-sulfonyl-D,L-Glu derivatives were studied by application of transferred NOE experiments. Nontrivial NOEs observed in transferred NOESY spectra show conformational dynamics of the ligands at the enzyme binding site that cannot be explored by X-ray diffraction. Conformational flexibility of the alkyloxy moiety and of the naphthalene ring is proposed. The preferred orientation of alkyloxy and D-Glu moieties relative to the naphthalene ring appears to be similar for all C6 substituted derivatives. Ligand epitope maps obtained by STD NMR technique indicate the importance of hydrophobic interactions and the segments of molecular structure that are responsible for them.

Unrestrained molecular dynamics simulations of ligand–MurD complexes clearly indicate the conformational flexibility of naphthalene-*N*-sulfonyl-D,L-Glu derivatives at the MurD binding site, which, in several examples described above, corresponds well with transfer NOE experiments and ligand epitope mapping and can be related to differences in ligand activities. Mutual dependence between naphthalene ring rotations and the conformational flexibility of its substituent were observed. The degree of conformational flexibility depends on the specificity of the ligand molecular structure and adaptability within the binding site. We were able to show the interplay between the hydrophobic and polar interactions and their possible effect on ligand affinity. We believe that the conclusions given above significantly upgrade the drug design studies that were based solely on the crystal structures.

In order to restate the reason for the differences in the activity of the studied compounds, we point out the crucial role of the nature of the naphthalene 6-substituent, which is a long spacer chain with an aromatic ring that potentiates hydrophobic interactions and, consequently, lowers the IC<sub>50</sub>. Having established the primary site of interaction and/or recognition at the binding site residing within the naphthalene *N*-sulfonyl-D,L-Glu fragment,<sup>3</sup> we believe we could achieve an affinity 2 orders of magnitude higher by designing appropriate hydrophobic moieties

as 6- or 7-naphthalene substituents that would also include sites for forming hydrogen bonds, as exemplified by the studied compounds.

## 4. Materials and Methods

**4.1. Isolation and Purification of MurD Enzyme from *E. coli*.** The protein was overexpressed and purified according to a slightly modified procedure for the 6× His-tag system previously described.<sup>13</sup> *E. coli* BL21-AI cells carrying the pABD16/MurD vector were grown at 37 °C in 2YT medium containing ampicillin (100 mg/L) to reach an  $A_{600\text{nm}}$  of approximately 1.0. Expression was induced with isopropyl  $\beta$ -D-thiogalactopyranoside (IPTG) at a final concentration of 1 mM and L-arabinose at a final concentration of 2 g/L. The growth was continued overnight at 25 °C. The cells were harvested and resuspended in buffer containing 20 mM potassium phosphate, 1 mM dithiothreitol, pH 7.2. The cells were lysed by ultrasound sonication. The suspension was centrifuged, and the pellet was discarded. Pre-equilibrated  $\text{Ni}^{2+}$ -nitrilotriacetate-agarose resin ( $\text{Ni}^{2+}$ -NTA) was added to the supernatant and incubated on a multifunction tube rotator for 1 h. The suspension was centrifuged to recover the resin. The protein was eluted with increasing concentrations of imidazole (20, 40, 100, and 300 mM) in buffer containing 50 mM potassium phosphate, 200 mM KCl, 1 mM dithiothreitol (DTT), pH 8. Fractions containing protein were collected and checked using SDS-PAGE electrophoresis. Fractions containing MurD protein with a satisfactory degree of purity were joined and concentrated using Amicon Ultra 10K NMWL concentrator. The buffer was exchanged with deuterated buffer containing 20 mM Tris (98%  $\text{D}_{11}$ ), 7 mM ammonium sulfate (98%  $\text{D}_8$ ), 3.5 mM  $\text{MgCl}_2$ , 0.3 mM DTT (98%  $\text{D}_{10}$ ), pD 7.2. The protein concentration was estimated by the Bradford method,<sup>14</sup> and the final concentration was determined by measuring  $A_{280}$  on a Nanodrop ND-1000 spectrophotometer. Deuterated glycerol was added to the protein solution as a cryoprotectant (10% v/v), and the solution was frozen at -30 °C. MurD activity was checked using a Biomol green assay.<sup>15</sup>

**4.2. Nuclear Magnetic Resonance.** The high-resolution NMR spectra were recorded on Varian INOVA 600 MHz and Varian DirectDrive 800 MHz spectrometers at 25 °C. All data were collected using pulse sequences provided in Varian libraries of pulse programs. Naphthalene-*N*-sulfonyl-D,L-glutamic acid derivatives were provided by Lek Pharmaceuticals d.d. Elemental analysis was used to determine the purity of compounds, which is  $\geq 95\%$ .<sup>3</sup> NMR samples were prepared in 99.9%  $\text{D}_2\text{O}$  buffer containing 20 mM Tris (98%  $\text{D}_{11}$ ), 7 mM  $(\text{ND}_4)_2\text{SO}_4$  (98%  $\text{D}_8$ ), 3.5 mM  $\text{MgCl}_2$ , 0.3 mM DTT (98%  $\text{D}_{10}$ ), and 0.4 mM ATP, pD 7.2. DSS (0.1 mM) was used as an internal standard. Protein concentrations were 0.034 and 0.018 mM, and ligand concentrations were 1.55 and 1.73 mM, depending on the type of NMR experiment. Samples were degassed using an ultrasound bath for 20 min.

STD ligand epitope mapping experiments<sup>10,11</sup> were performed at 800 MHz with a 10 000 Hz spectral width, 16 384 data points, saturation time of 350 ms, and 10000–15000 scans. Relaxation time was 4.5 or 5.5 s depending on the longest  $^1\text{H}$   $T_1$  relaxation time of a particular derivative. Spectra were recorded at an enzyme/ligand ratio of 1:97. Selective saturation was achieved by a train of 50 ms long Gauss-shaped pulses separated by a 1 ms delay. Water was suppressed via excitation sculpting.<sup>16,17</sup> The on-resonance selective saturation of the enzyme was applied at 0.21 or at -0.17 ppm depending on the position of proton resonances of the naphthalene substituents. Off-resonance irradiation was applied at 30 ppm for the reference spectrum. Subtraction of on- and off-resonance spectra was performed internally via phase cycling. Spectra were zero-filled twice and apodized by an exponential line broadening function of 1 Hz.

Inversion recovery  $T_1$  experiments were recorded at 800 MHz with an 8390 Hz  $^1\text{H}$  spectral width, 16 384 data points, 40 scans, and a relaxation delay of 16 s. Ligand concentrations were 0.2 mM.

Values of  $T_1$  relaxation times were determined from nine spectra recorded with recovery delays ranging from 0.06 to 16 s.

The transferred NOESY<sup>7,8</sup> spectra were acquired at an enzyme/ligand ratio of 1:45 with 4096 data points in  $t_2$ , 64–128 scans, 256–356 complex points in  $t_1$ , mixing time of 250 ms, and a relaxation delay of 1.5 s. The  $^1\text{H}$  sweep widths were 6010 and 8278 Hz at 600 and 800 MHz, respectively. The residual water signal was suppressed using excitation sculpting,<sup>16,17</sup> and adiabatic pulses<sup>18</sup> were applied for suppression of zero quantum artifacts during mixing time.  $T_1\rho$  filter of 30 ms was used to eliminate the background protein resonances. Spectra were processed and analyzed with FELIX 2002 software package from Accelrys Software Inc. Spectra were zero-filled twice and apodized with a squared sine bell function shifted by  $\pi/2$  in both dimensions. Cross-peak volumes in NOESY spectra were calculated using an integration routine within the FELIX software. Distances were calculated from cross-peak volumes using the two-spin approximation and the integrated intensity of a pair of protons H1 and H8 in the naphthalene ring assumed to have a distance of 2.46 Å.

**4.3. Molecular Dynamics.** All the calculations were performed on Beowulf-type CROW clusters<sup>19</sup> at the National Institute of Chemistry in Ljubljana, Slovenia, utilizing the CHARMM molecular modeling suite,<sup>20</sup> developmental version 36a1. Starting coordinates were obtained from the Protein Data Bank: PDB entries 2JFH for compound **20**, 2JFF for compound **17c**, and 2UUP for compound **17l**. Since all compounds share a common D-Glu moiety, sulfonamide group, naphthalene ring, and ether oxygen, starting coordinates for those parts for compounds **17f**, **17g**, **17k**, **17i**, and **17j** were obtained from those of compound **17l**. Missing atoms were constructed using internal coordinates in CHARMM. Hydrogen atoms were added using the CHARMM HBUILD routine. Force field parameters were obtained from the CHARMM parameter and topology files (version 27) for proteins.<sup>21,22</sup> Since no satisfactory parameters for the sulfonamide group were available from the CHARMM parameter files, vibration frequencies were calculated using quantum mechanical methods via the Gaussian 03 program. Parameters for the sulfonamide group in CHARMM were adjusted to match vibration frequencies calculated in Gaussian 03. Charges for sulfonyl oxygens and ether oxygen were refined by adding water molecules and calculating interaction energy using Gaussian 03. CHARMM parameters were adjusted to obtain the same interaction energy as energy calculated ab initio in Gaussian 03. The compounds alone were subjected to energy minimization using adopted basis Newton–Raphson method using 1000 steps and then hydrated by immersion into a cubic box ( $86 \text{ \AA} \times 86 \text{ \AA} \times 86 \text{ \AA}$ ) of water molecules. Deletion of water molecules overlapping with the protein resulted in a system with approximately 20 000 TIP3 water molecules. The entire system was again subjected to energy minimization using the adopted basis Newton–Raphson method using 1000 steps. Molecular dynamics simulations were run at 1 fs time steps for 2 ns. CPT ensemble was used in all calculations with a pressure of 1 bar and temperature of 300 K. Electrostatic interactions were computed with the particle-mesh Ewald method. A VMD program was used for visualization of MD simulations.<sup>23</sup>

**Acknowledgment.** This work was supported by the Ministry of Higher Education, Science and Technology of Slovenia (Grants J1-0317-0104-08 and P1-0010), Lek Pharmaceuticals d.d., and the European Union FP6 Integrated Project EUR-INTAFAR (Project LSHM-CT-2004-512138) under the thematic priority Life Sciences, Genomics and Biotechnology for Health.

**Supporting Information Available:** Tables of  $^1\text{H}$  chemical shift assignments, ligand distances, dihedral angles, and ligand–enzyme distances from MD trajectories and snapshots from MD trajectories. This material is available free of charge via the Internet at <http://pubs.acs.org>.

## References

- (1) van Heijenoort, J. Recent advances in the formation of the bacterial peptidoglycan monomer unit. *Nat. Prod. Rep.* **2001**, *18*, 503–519.



- (2) Barreateau, H.; Kovac, A.; Boniface, A.; Sova, M.; Gobec, S.; Blanot, D. Cytoplasmic steps of peptidoglycan biosynthesis. *FEMS Microbiol. Rev.* **2008**, *32*, 168–207.
- (3) Humljan, J.; Kotnik, M.; Contreras-Martel, C.; Blanot, D.; Urleb, U.; Dessen, A.; Šolmajer, T.; Gobec, S. Novel naphthalene-*N*-sulfonyl-D-glutamic acid derivatives as inhibitors of MurD, a key peptidoglycan biosynthesis enzyme. *J. Med. Chem.* **2008**, *51*, 7486–7494.
- (4) Kotnik, M.; Humljan, J.; Contreras-Martel, C.; Oblak, M.; Kristan, K.; Herve, M.; Blanot, D.; Urleb, U.; Gobec, S.; Dessen, A.; Šolmajer, T. Structural and functional characterization of enantiomeric glutamic acid derivatives as potential transition state analogue inhibitors of MurD ligase. *J. Mol. Biol.* **2007**, *370*, 107–115.
- (5) Pratiel-Sosa, F.; Acher, F.; Trigalo, F.; Blanot, D.; Azerad, R.; van Heijenoort, J. Effect of various analogues of D-glutamic acid on the D-glutamate-adding enzyme from *Escherichia coli*. *FEMS Microbiol. Lett.* **1994**, *115*, 223–228.
- (6) Teague, S. J. Implications of protein flexibility for drug discovery. *Nat. Rev. Drug Discovery* **2003**, *2*, 527–541.
- (7) Clore, G. M.; Gronenborn, A. M. Theory and applications of the transferred nuclear Overhauser effect to the study of the conformations of small ligands bound to proteins. *J. Magn. Reson.* **1982**, *48*, 402–417.
- (8) Clore, G. M.; Gronenborn, A. M. Theory of the time dependent transferred nuclear Overhauser effect: applications to structural analysis of ligand–protein complexes in solution. *J. Magn. Reson.* **1983**, *53*, 423–442.
- (9) Mayer, M.; Meyer, B. Characterization of ligand binding by saturation transfer difference NMR spectroscopy. *Angew. Chem., Int. Ed.* **1999**, *38*, 1784–1788.
- (10) Mayer, M.; Meyer, B. Group epitope mapping by saturation transfer difference NMR to identify segments of a ligand in direct contact with a protein receptor. *J. Am. Chem. Soc.* **2001**, *123*, 6108–6117.
- (11) Yan, J.; Kline, A. D.; Mo, H.; Shapiro, M. J.; Zartler, E. R. The effect of relaxation on the epitope mapping by saturation transfer difference NMR. *J. Magn. Reson.* **2003**, *163*, 270–276.
- (12) Bertrand, J. A.; Auger, G.; Martin, L.; Fanchon, E.; Blanot, D.; Le Beller, D.; van Heijenoort, J.; Dideberg, O. Determination of the MurD mechanism through crystallographic analysis of enzyme complexes. *J. Mol. Biol.* **1999**, *289*, 579–590.
- (13) Bouhss, A.; Dementin, S.; Parquet, C.; Mengin-Lecreux, D.; Bertrand, J. A.; Le Beller, D.; Dideberg, O.; van Heijenoort, J.; Blanot, D. Role of the ortholog and paralog amino acid invariants in the active site of the UDP-MurNac-L-alanine:D-glutamate ligase (MurD). *Biochemistry* **1999**, *38*, 12240–12247.
- (14) Bradford, M. M. A rapid and sensitive method for the quantitation of microgram quantities of protein utilizing the principle of protein–dye binding. *Anal. Biochem.* **1976**, *72*, 248–254.
- (15) Bratkovic, T.; Lunder, M.; Urleb, U.; Strukelj, B. Peptide inhibitors of MurD and MurE, essential enzymes of bacterial cell wall biosynthesis. *J. Basic Microbiol.* **2008**, *48*, 202–206.
- (16) Hwang, T. L.; Shaka, A. J. Water suppression that works. Excitation sculpting using arbitrary wave-forms and pulsed-field gradients. *J. Magn. Reson., Ser. A* **1995**, *112*, 275–279.
- (17) Dalvit, C. Efficient multiple-solvent suppression for the study of the interactions of organic solvents with biomolecules. *J. Biomol. NMR* **1998**, *11*, 437–444.
- (18) Thrippleton, M. J.; Keeler, J. Elimination of zero-quantum interference in two-dimensional NMR spectra. *Angew. Chem., Int. Ed.* **2003**, *42*, 3938–3941.
- (19) Borstnik, U.; Hodoscek, M.; Janezic, D. Improving the performance of molecular dynamics simulations on parallel clusters. *J. Chem. Inf. Comput. Sci.* **2004**, *44*, 359–364.
- (20) Brooks, B. R.; Bruccoleri, R. E.; Olafson, B. D.; States, D. J.; Swaminathan, S.; Karplus, M. CHARMM: a program for macromolecular energy, minimization, and dynamics calculations. *J. Comput. Chem.* **1983**, *4*, 187–217.
- (21) MacKerell, A. D.; Bashford, D.; Bellott, M.; Dunbrack, R. L.; Evanseck, J. D.; Field, M. J.; Fischer, S.; Gao, J.; Guo, H.; Ha, S.; Joseph-McCarthy, D.; Kuchnir, L.; Kuczera, K.; Lau, F. T. K.; Mattos, C.; Michnick, S.; Ngo, T.; Nguyen, D. T.; Prodhom, B.; Reiher, W. E.; Roux, B.; Schlenkrich, M.; Smith, J. C.; Stote, R.; Straub, J.; Watanabe, M.; Wiorkiewicz-Kuczera, J.; Yin, D.; Karplus, M. All-atom empirical potential for molecular modeling and dynamics studies of proteins. *J. Phys. Chem. B* **1998**, *102*, 3586–3616.
- (22) MacKerell, A. D.; Feig, M.; Brooks, C. L. Extending the treatment of backbone energetics in protein force fields: limitations of gas-phase quantum mechanics in reproducing protein conformational distributions in molecular dynamics simulations. *J. Comput. Chem.* **2004**, *25*, 1400–1415.
- (23) Humphrey, W.; Dalke, A.; Schulten, K. VMD: visual molecular dynamics. *J. Mol. Graphics* **1996**, *14*, 33–38.

JM900117N